Research Article

Qian Bai*, Ziliang Chen, Yingming Gao, Hang Li, and Jingang Tang

Residual stress relaxation considering microstructure evolution in heat treatment of metallic thin-walled part

https://doi.org/10.1515/htmp-2022-0036
received February 16, 2022; accepted April 18, 2022

Abstract: The forming-induced residual stress of metallic parts could cause undesired deformation in the final machining process, especially for the thin-walled parts. Therefore, heat treatment is essential to release the residual stress prior to machining. This study investigates the residual stress change of a forged pure iron part in annealing heat treatment and material removal processes. A modified creep constitutive model with the consideration of microstructure evolution was established to describe the residual stress relaxation in the annealing. Stress relaxation tests were conducted to calibrate the material constants. This constitutive model was then implemented into the finite element model of annealing for the cold-forged semi-spherical shell. The residual stress and the grain size of the shell were predicted at different heating temperatures. The semi-spherical shells were machined to the final thin-walled parts, and the deformation owing to the residual stress release was measured and compared to the simulation results. The heating temperature was determined aiming to minimize the machining-induced deformation as well as to ensure the microstructure. This study could provide guidance to the elimination of the residual stress and the improvement of the geometrical accuracy for thin-walled parts in the machining process.

Keywords: thin-walled part, residual stress relaxation, dislocation density, microstructure evolution, deformation prediction

*** Corresponding author: Qian Bai,** Key Laboratory for Precision and Non-traditional Machining Technology of Ministry of Education, Dalian University of Technology, Dalian 116024, China, e-mail: baiqian@dlut.edu.cn
Ziliang Chen, Yingming Gao, Hang Li: Key Laboratory for Precision and Non-traditional Machining Technology of Ministry of Education, Dalian University of Technology, Dalian 116024, China
Jingang Tang: Institute of Mechanical Manufacturing Technology, China Academy of Engineering Physics, Mianyang 621900, China

1 Introduction

Thin-walled parts have great significance in reducing weight and improving the performance of the components. The forming processes of these thin-walled parts mainly include casting, forging, welding, and additive manufacturing, in which large residual stress could be generated. In the subsequent machining process, the release and redistribution of this residual stress, as one of the main reasons for the part deformation owing to the weak rigidity, deteriorates the geometrical accuracy of the parts [1]. Therefore, the measures to eliminate the forming-induced residual stress are essential prior to machining.

Many methods have been developed to reduce the forming-induced residual stress, such as heat treatment, vibration aging, and cryogenic treatment, among which annealing heat treatment is widely used for its advantages of high efficiency and convenience. Since various forming processes cause different residual stress distributions, the heat treatment parameters are normally determined by trial-and-error tests. Some researchers developed empirical models to predict the stress change in the annealing for the parts fabricated by shot peening [2,3], additive manufacturing [4], and cutting [5]. However, it was a lack of mechanism interpretation in these empirical models. Classical creep models take into account the effects of initial strain hardening of the parts and have been applied to explain the residual stress relaxation in the annealing for the parts fabricated by shot peening [6], welding [7–9], coating [10], and cold-rolling [11]. In the process of heat treatment, due to the initial strain hardening and high-temperature conditions of the parts, recovery and recrystallization may occur. However, the microstructure is supposed to maintain the optimal state, accompanied by the residual stress relaxation after the annealing heat treatment. Therefore, in order to determine the annealing parameters to achieve the required microstructure and residual stress, it is necessary to

develop a residual stress prediction modeling considering microstructure evolution in heat treatment.

Stress measurement is needed to verify the prediction of the residual stress of a part. Normally, residual stress can be measured by hole drilling method, ring core method, and diffraction method. Among these methods, the measurement accuracy of hole drilling is around ±50 MPa under ideal conditions [12]. The basic principle of the ring core method is similar to that of the hole drilling method, but the accuracy is usually higher than the hole drilling method, which may reach the value of ±15 MPa [13]. The X-ray diffraction (XRD) method is the most commonly used method with a measurement accuracy of ±20 MPa [14]. After heat treatment, the absolute value of residual stress is small [15]. As a result, it is difficult to measure the residual stress accurately by using the aforementioned methods. The deformation of thin-walled components after machining is usually caused by the initial residual stress [16,17]. Therefore, the residual stress with a small absolute value can be evaluated by using the deformation of low-stiffness parts after machining.

In this article, a stress relaxation model considering microstructure evolution was established to predict microstructure evolution and residual stress relaxation during heat treatment. The residual stress after heat treatment was evaluated by measuring the deformation of the parts after material removal. The accuracy of the proposed stress relaxation model was verified by comparing the microstructure prediction with the measured results.

2 Experimental procedures

The stress relaxation tests were conducted to study the stress change at annealing temperatures. The initial strain hardening affects the residual stress relaxation during the heat treatment. As a result, the rolling process was carried out to introduce different initial strain levels in the stress relaxation test samples, as shown in Figure 1. Three pure iron plates with a diameter of 180 mm and a height of 50 mm were cold-rolled to heights of 40, 30, and 20 mm, respectively. These three cold-rolled plates had different initial strains of 0.22, 0.51, and 0.91, respectively. Cylindrical samples (Figure 1(b)) were then obtained by wire cutting and turning for the stress relaxation tests. The initial grain size was 45 μm.

In the proposed stress relaxation model in this article, dislocation density was involved to describe the stress change during annealing. The initial dislocation densities of the rolled iron plates were measured using an Empyrean

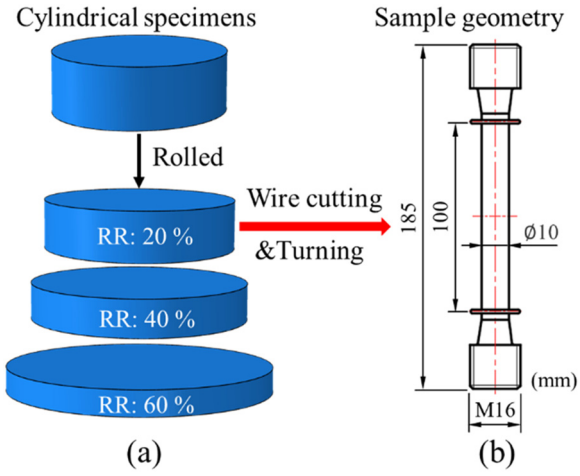

Figure 1: (a) Cold-rolled pure iron plates; (b) dimension of the stress relaxation test samples.

XRD instrument with Co-target. Bragg diffraction angle was 20–130°, and the angle step was 0.013°. The tube current was 40 mA with a tube voltage of 40 kV. The experimental data were analyzed using Jade. 5 software. Initial dislocation density was calculated from the diffraction pattern (Figure 2) with the Williamson equation:

$$\rho = \frac{2\sqrt{3}\langle \varepsilon_m^2 \rangle^{1/2}}{bD}, \tag{1}$$

where D is the crystallite size, and $\langle \varepsilon_m^2 \rangle^{1/2}$ is the root-mean-square of micro-strain. These two parameters can be calculated as follows:

$$\varepsilon_m = \frac{0.89\lambda}{F \cos\theta}, \tag{2}$$

$$D = \frac{\lambda}{F \tan\theta}, \tag{3}$$

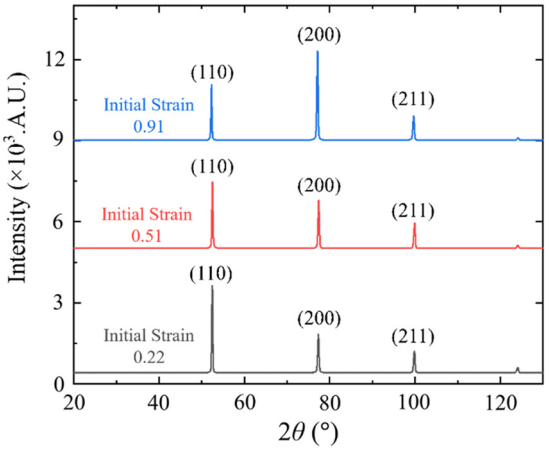

Figure 2: XRD patterns of the samples with different initial strains.

Table 1: Process parameters of heat treatment

Initial strain	Heat treatment temperature T (°C)	Holding time t (min)
0.22	650	0–360
	700	
	800	
0.51	650	0–240
	700	
	800	
0.91	650	0–120
	700	
	800	

where F is the full width at half maximum of peaks, θ is the Bragg angle, and λ is the diffraction wavelength, and for Co-Kα radiation, $\lambda = 1.78901$ Å.

The heat treatment experiments were carried out in a furnace (SG-XQL1200, Shanghai Institute of Optics and Fine Mechanics, Chinese Academy of Sciences, China). In order to study the microstructure evolution during the annealing, the grain size was observed after different heating times and temperatures. Cubic samples were cut from rolled plates with different initial strains. Subsequently, heat treatment was performed as shown in Table 1. After the heat treatment, the samples were polished and etched in a solution of nitric acid (4 mL) and C_2H_5OH (100 mL) at ambient temperature for 30 s. Optical microscopy observations and Vickers hardness measurements were carried out.

The stress relaxation experimental procedure included three stages: heating stage, loading stage, and constant strain stage. The temperature and load profiles in the stress relaxation test are shown in Figure 3(a). In stage I, the samples were heated to test temperatures (i.e., 500, 600, and 650°C) at a heating rate of 0.5°C·s^{-1}. In stage II, the samples were held at the test temperatures for 5 min; in the meantime, the load was increased at a loading speed of 0.583 MPa·s^{-1}. In stage III, a constant strain was held. With the increased time, the stress was released. The stress relaxation tests were conducted in a stress relaxation testing machine of RDL-50, according to the GB/T 2039–2012 standard (Figure 3(b)).

Thin-walled pure iron spherical shell parts were fabricated as shown in Figure 4. First, pure iron plates with a diameter of 385 mm and a thickness of 23 mm were cold-forged to obtain the semi-spherical shells, and the maximum load during the forging process was 170 tons (Figure 4(a)). The thickness of the shell was 22 mm, and the inner diameter was 236 mm (Figure 4(b)). Then, the heat treatment annealing was conducted for the shells with a temperature of 650°C and a holding time of 4 h. Finally, the shells were machined by turning to fabricate the final parts (Figure 4(c)). The final thickness of the part was 2.4 mm, indicating the low stiffness feature of the part.

3 Residual stress relaxation model

The residual stress in cold-forged parts is mainly produced by uneven plastic deformation in the forging process. As shown in equation (4), the total strain (ε_{tot}) consisting of elastic strain (ε_e), plastic strain (ε_{pl}), and creep strain (ε_c) remains constant [18]. During the heat treatment process, the residual elastic strain of the metal material changes to creep strain, and thus, the residual stress gradually decreases.

$$E_{tot} = \varepsilon_e + \varepsilon_{pl} + \varepsilon_c, \tag{4}$$

$$\dot{\varepsilon}_e = -\dot{\varepsilon}_c = -\frac{d\sigma}{E \cdot dt}. \tag{5}$$

The creep strain rate ε_c can be calculated with the classic power law creep model [19]:

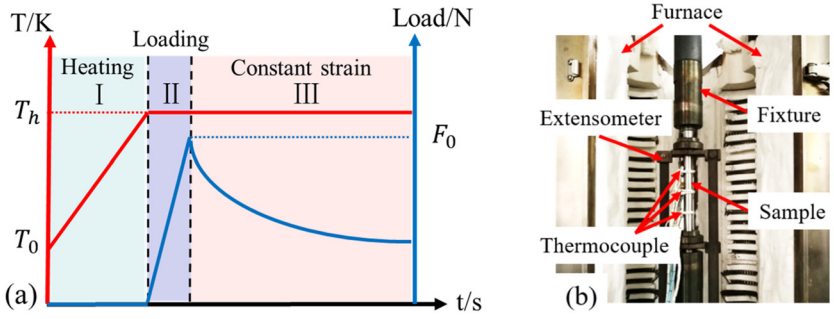

Figure 3: (a) Schematic of stress relaxation test procedures; (b) stress relaxation testing machine.

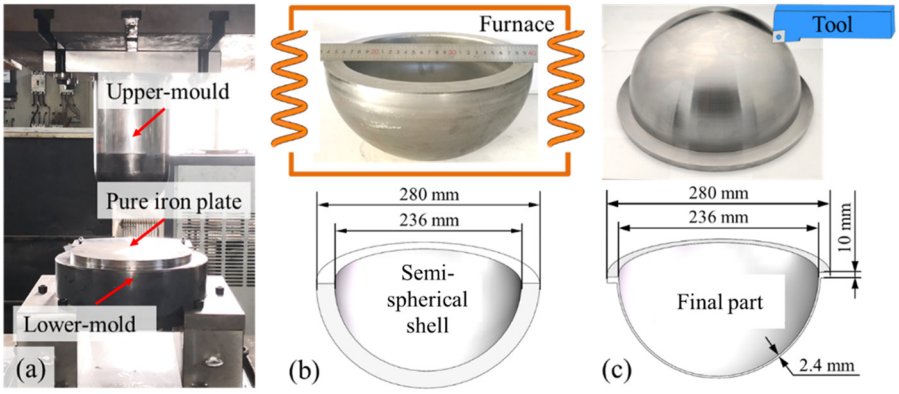

Figure 4: (a) Cold-forging process; dimensions of (b) cold-forged semi-spherical shell; and (c) final part machined by turning.

$$\dot{\varepsilon}_c = \dot{\varepsilon}_0 \left(\frac{\sigma}{\hat{\sigma}}\right)^n, \tag{6}$$

where σ is the residual stress, $\hat{\sigma}$ is the slip resistance of dislocation, and $\dot{\varepsilon}_0$ is the critical strain rate, which can be expressed as

$$\dot{\varepsilon}_0 = A \exp\left(-\frac{Q}{RT}\right), \tag{7}$$

where A is the material constant, Q is the activation energy, R is the gas constant, and T is the heat treatment temperature.

In equation (6), n is the material constant which is dependent on the extent of plastic deformation [18]:

$$n = n_0(2 - \exp(-B\varepsilon_{\text{ini}})), \tag{8}$$

where n_O and B are the material constants and ε_{ini} is the initial strain.

The slip resistance of dislocation $\hat{\sigma}$ is expressed in terms of the dislocation density ρ [19]:

$$\hat{\sigma} = M\alpha G b\sqrt{\rho}\ , \tag{9}$$

where M is the average Taylor factor, b is the Burgers vector, and the shear modulus G is dependent on the temperature and can be written as [20]:

$$G = G_0\left(1 - 0.81\frac{T - 300}{T_m}\right), \tag{10}$$

where G_0 is a temperature-dependent constant, T is the heat treatment temperature, and T_m is the melting temperature.

During the process of stress relaxation, the evolution of dislocation density is related to the initial hardening, the recovery, and the static recrystallization. The variation of ρ in the process of creep at high temperatures is described as equation (11) [21,22].

$$\dot{\rho} = k_1\dot{\varepsilon}_c\sqrt{\rho} - k_2\dot{\varepsilon}_c^m\rho\exp\left(-\frac{Q}{RT}\right) - k_3\rho^l\exp\left(-\frac{Q}{RT}\right) - \frac{k_4\rho\dot{X}_{\text{srex}}}{1 - X_{\text{srex}}}, \tag{11}$$

where X_{srex} represents the volume fraction of recrystallization, and it can be calculated using Avrami model [23,24]; k_1, k_2, m, k_3, l, and k_4 are the material constants.

Generally, the kinetics of recrystallization is expressed by the Avrami equation as follows:

$$X_{\text{srex}} = 1 - \exp\left(-\beta\left(\frac{t}{t_{0.5}}\right)^{k_s}\right), \tag{12}$$

$$t_{0.5} = a_3 d_0^{h_3}\varepsilon^{n_3}\exp\left(\frac{Q_3}{RT}\right), \tag{13}$$

where $t_{0.5}$ is a characteristic time for recrystallization corresponding to $X_{\text{srex}} = 0.5$, d_0 is the initial grain size, ε is the initial strain, Q_3 is the activation energy of the recrystallization, and R is the gas constant.

The recrystallized volume fraction, X_{srex}, is calculated based on Vickers hardness measurements [25]:

$$X_{\text{srex}} = \frac{HV_{\text{initial}} - HV(t)}{HV_{\text{initial}} - HV_{\text{final}}}, \tag{14}$$

where HV_{initial} is the initial hardness of compressed samples before heat treatment, $HV(t)$ is the instantaneous hardness after holding time t, and HV_{final} is the hardness after recrystallization.

Different initial strains and heat treatment conditions have great effects on the microstructure evolution. Figure 5 shows the microstructure of pure iron samples with different initial strains after heat treatments. With the increase in the heat treatment temperature and the initial strain, the volume fraction of the crystallization was increased. It is attributed to the fact that the stored strain energy generated

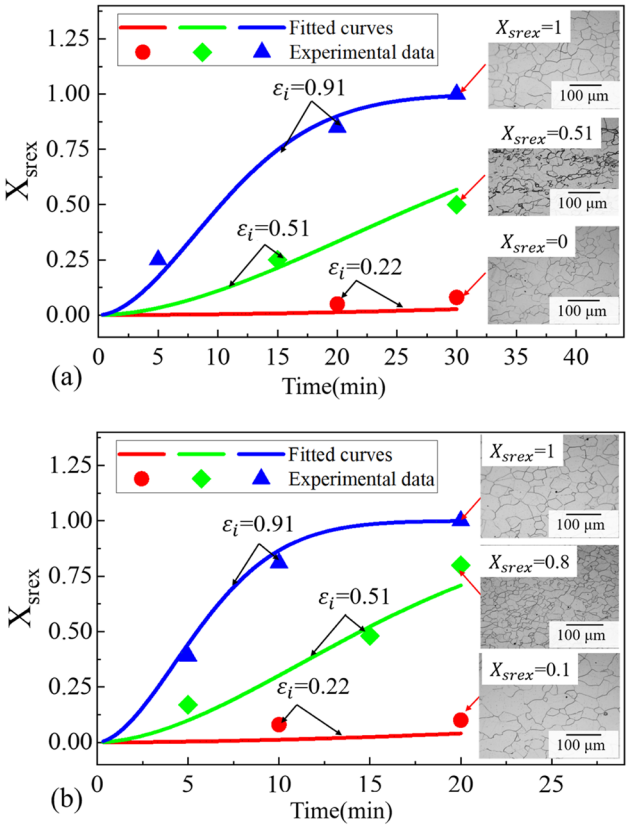

Figure 5: Experimental data and fitted curves of volume fraction of recrystallization (X_{srex}) at temperatures of (a) 923 K and (b) 973 K.

from cold-forging was the driving force for the recrystallization, and the high temperature enhanced the velocity of grain boundary migration to accelerate the recrystallization process. Micro-hardnesses of these samples were measured to calibrate the parameters in the Avrami model in equation (12). The fitted parameters are shown in Table 2. The fitted curves of the volume fraction of recrystallization are in good agreement with the experimental data, which indicates that the calibrated Avrami model was validated to predict the microstructure evolution in the annealing heat treatment.

Based on the stress relaxation experimental results, the fitted parameters of the stress relaxation model are calibrated as shown in Table 3. The stress relaxation experimental and fitted results are plotted in Figure 6. The stress of the samples with different initial strains decreases rapidly at a temperature between 873 and 963 K. Since the dislocation density in the material was decreased during the annealing, the decreasing rate of residual stress gradually slowed down until it finally reached a relatively stable value.

Table 2: Fitted parameters in the Avrami model

β (–)	k_s (–)	a_3 (–)	h_3 (–)	n_3 (–)	Q_3 (J)
1,250	1.78	5.8×10^{-4}	0.4	−2.15	125,000

Figure 6(a) shows the stress dropped to 49, 36, and 25 MPa at 923 K for the samples with the initial strain of 0.22, 0.51, and 0.91, respectively. With a higher initial strain, the residual stress is reduced faster due to more mobile dislocations generated by the initial hardening. In addition, the recrystallization occurred in the samples with the initial strain of 0.91 at 923 K in Figure 5, which eliminated the dislocations and accelerated the stress drop.

Figure 6(b) shows the normalized stress change for the samples with the initial strain of 0.22 at different temperatures of 873, 923, 943, and 963 K, respectively. It indicates that the relaxation behavior of the cold-rolled samples had temperature sensitivity. For samples with the initial strain of 0.22, the thermal activation at a lower temperature was insufficient to start the stress relaxation completely. By contrast, with the increase in the heating temperature, the thermal activation was increased, which led to a significant decrease in stress.

4 Finite element (FE) model of forging, annealing, and material removal processes

A three-dimensional FE model was developed using the commercial software ABAQUS to predict the residual stress and deformation of the thin-walled part in the cold-forging, heat treatment, and material removal processes. The FE model of the cold-forging process (Figure 7(a)) consisted of rigid molds and a deformable blank. The element type of the part was C3D8R with a size of 2 mm × 2 mm × 2 mm.

Table 3: Fitted parameters in the stress relaxation model

A (–)	Q (J)	n_0 (–)	B (–)	k_1 (–)	k_2 (–)	m (–)	k_3 (–)	l (–)	k_4 (–)
1.2×10^9	444,500	9.3	0.39	1.2×10^5	0.04	−3.5	1×10^4	2.26	0.8

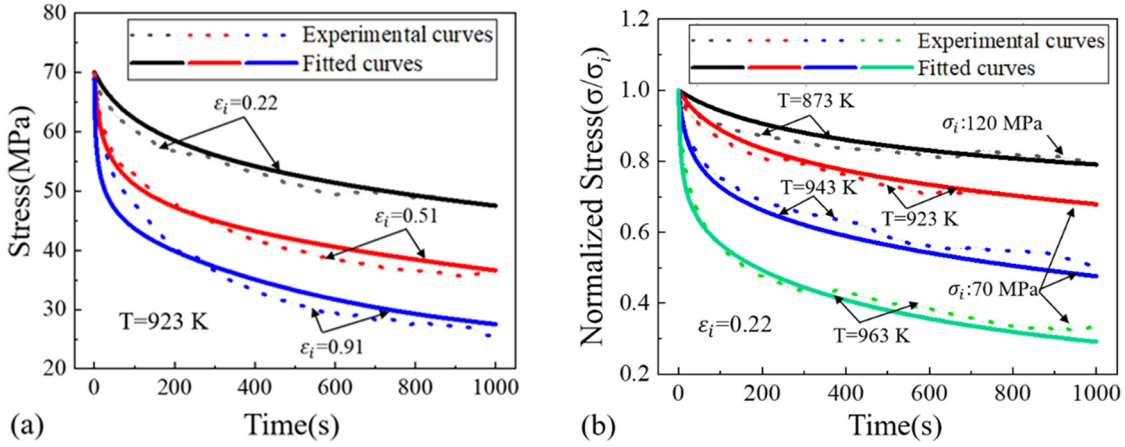

Figure 6: Experimental and fitted curves of the stress relaxation with (a) different initial strains; (b) different heat treatment temperatures.

The movement velocity of the upper mold was 12 mm·s^{-1}. In this model, the material of the workpiece was assumed isotropic, Poisson's ratio was 0.34, and Young's modulus was calculated in equation (10). The residual stress and plastic strain distribution in the semi-spherical shell were obtained from the cold-forging FE analysis. Then, the annealing heat treatment was simulated to predict the stress relaxation of the cold-forged semi-spherical shell (Figure 7(b)). The proposed stress relaxation model was implemented in the user-defined subroutine CREEP. The heat treatment temperature in the FE analysis was set at 500, 600, and 650°C, respectively. The evolution of residual stress and grain size in the shell during heat treatment was obtained. Finally, the material removal process was simulated to obtain the final part by using the element birth and death method (Figure 7(c)). The final residual stress distribution and the part deformation caused by the release of the residual stress were predicted and compared with the experimental results.

5 Results and discussion

5.1 Residual stress distribution

The simulated residual stress distributions of the semi-spherical shells after cold-forging and after annealing are shown in Figure 8. After forging, the maximum principal stress was compressive in the inner surface. From the inner surface to the outer surface, the compressive residual stress was increased to the maximum value of −335.8 MPa and then transformed into tensile stress of 196.4 MPa.

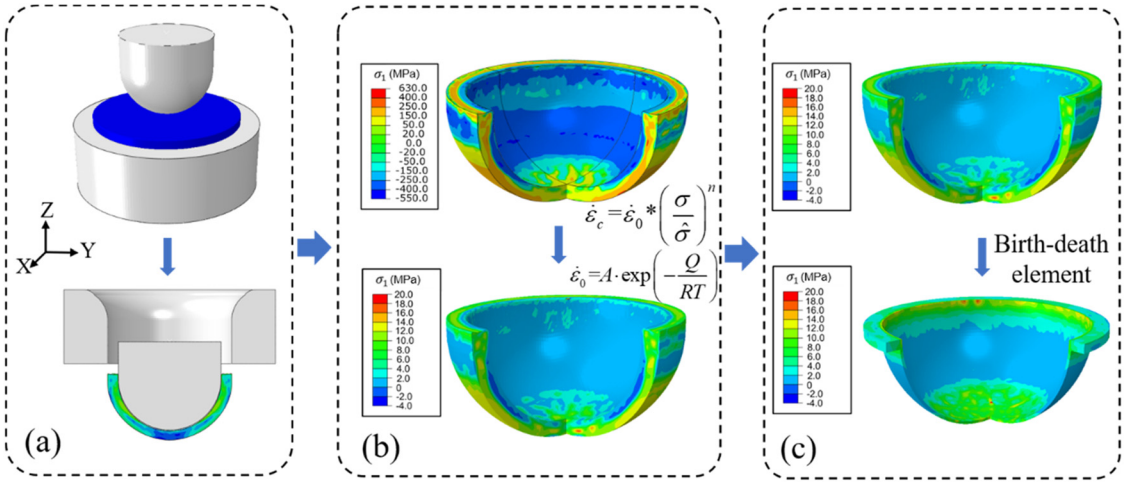

Figure 7: FE model of (a) cold-forging, (b) annealing heat treatment, and (c) material removal processes.

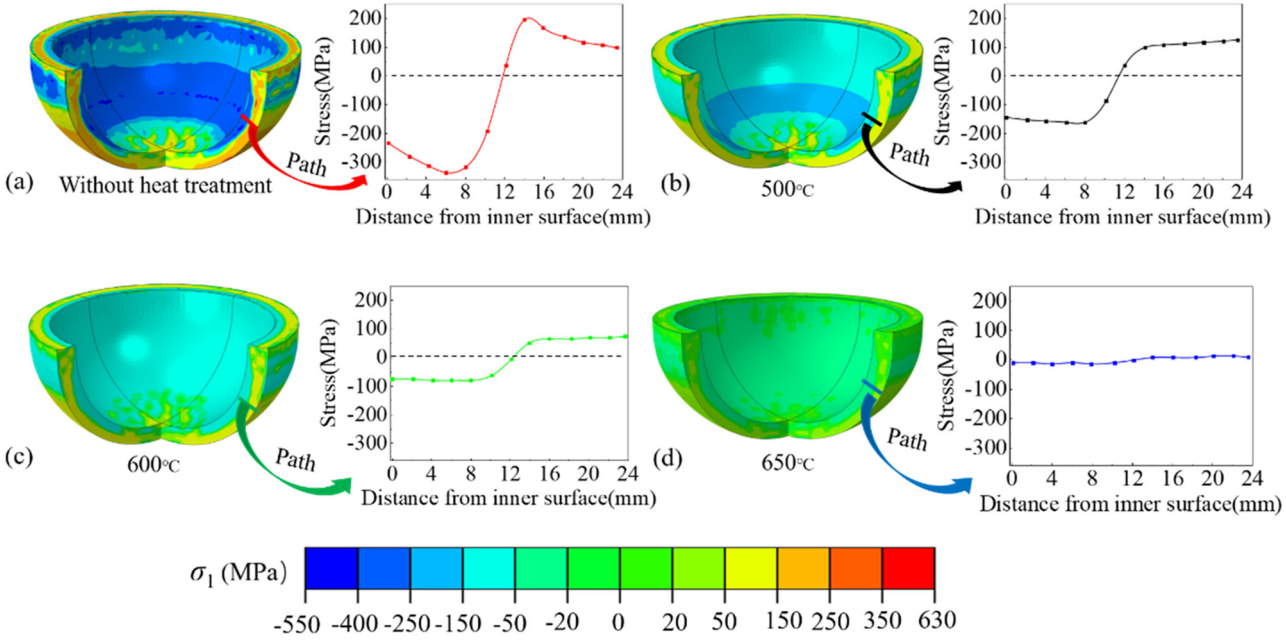

Figure 8: Residual stress distributions (a) after cold-forging, and after annealing at (b) 500°C, (c) 600°C, and (d) 650°C.

In general, the residual stress remaining in the workpiece was due to the uneven elastoplastic deformation. During the process of the cold-forging, the deformation was mainly concentrated on the surfaces of the part, i.e., the inner surface was squeezed and the outside surface was stretched. After forging, the elastic deformation remaining on the surface had the trend of recovering to the original state. However, the material inside the part hindered the recovery of the material on the surface. As a result, the stress at the inner surface was compressive, and the stress at the outside surface was tensile. On the one hand, the state of residual stress after heat treatment was the same as that after cold-forging. With the increase in the annealing temperature, the residual stress in the semi-spherical shell decreased obviously (Figure 8(b–d)) and reached a value between −20 and 20 MPa at 650°C. Therefore, the influence of residual stress on the final part deformation could be reduced.

5.2 Grain size distribution

Figure 9 shows the grain size distributions of the semi-spherical shell at different annealing temperatures. The initial grain size was 45 μm. As shown in Figure 9(a), with an annealing temperature of 650°C, the recrystallization occurred at the top of the semi-spherical shell, and thus, the grain size was decreased to 33.7 μm. Little recrystallization occurred in most other areas. As shown in Figure 9(b), with an annealing temperature of 700°C, recrystallization and grain growth occurred in a larger area. The largest grain size reached 139 μm due to a higher temperature, which resulted in an uneven distribution of the grain size in the semi-spherical shell.

To verify the microstructure prediction results of the cold-forging and heat treatment simulation, the experimental and predicted results of grain size were analyzed. The simulated grain size distribution of the semi-spherical shell after 650°C heat treatment is shown in Figure 10(a). Four areas in the section were selected for microstructure observation. The microstructure metallographic images of these areas after heat treatment were obtained using Olympus metallographic microscope, as shown in Figure 10(b). By comparing the

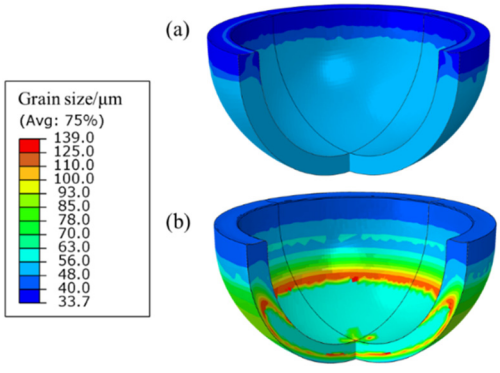

Figure 9: Grain size distributions of the semi-spherical shell at annealing temperatures of (a) 650°C and (b) 700°C.

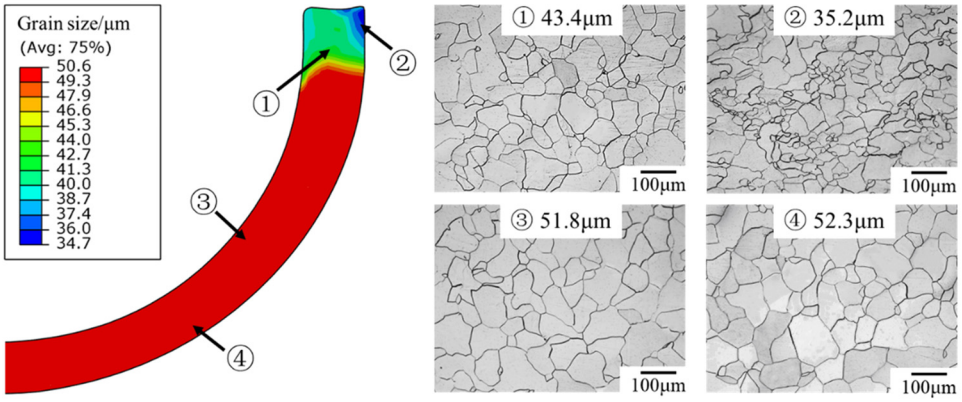

Figure 10: (a) Simulated results of grain size; (b) microstructure images and average grain size at 650°C.

results in Figure 10(a) and (b), the predicted grain size distribution of the stress relaxation model based on dislocation density was validated.

5.3 Deformation of the final part

In this study, the thin-walled spherical shell was machined to achieve the final part. The machining setup is shown in Figure 11. The semi-spherical shell was mounted onto the jaw chuck of a lathe machine. The machining process of thin-walled parts was divided into three steps, i.e., roughing, semi-finishing, and finishing steps, respectively. The machining parameters for these three steps are shown in Table 4.

Since the very small residual stress was difficult to measure using conventional method, the deformation after material removal was measured to verify the prediction results. The outer surface profile of the final part was measured using a coordinate measuring machine. The measuring paths shown in Figure 12(a) were parallel to the horizontal plane. The measured profile of the outer surface in the Cartesian absolute coordinate system is shown in Figure 12(c) and (d). It is found that the deformation value of the final part without heat treatment was larger than that with 650°C heat treatment. This phenomenon indicates that annealed part was not prone to deform, which was caused by the residual stress relaxation during heat treatment.

Table 4: Machining parameters of thin-walled parts

	Cutting speed ($m \cdot min^{-1}$)	Feed rate ($mm \cdot r^{-1}$)	Cutting depth (mm)
Roughing	120	0.15	0.5
Semi-finishing	120	0.1	0.2
Finishing	100	0.06	0.1

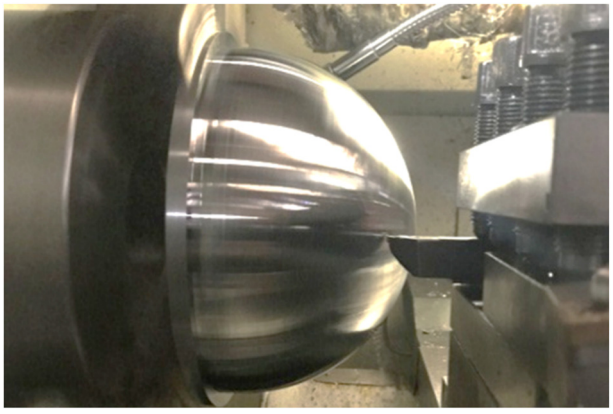

Figure 11: Machining setup of thin-walled parts.

In the FE simulation of the material removal process, different residual stress distributions were obtained after heat treatments for semi-spherical shells. Subsequently, the material allowance was removed using the birth–death element method, and the deformation of the final part caused by the residual stress release was calculated. The deformation along the radial direction is shown in Figure 13. The deformation of the final part presents a centrosymmetric distribution. The flange area shrunk inward, while the other areas extended outward along the radial direction.

Based on the developed FE model of forging, heat treatment, and material removal processes, the effect of annealing temperature on the residual stress-induced deformation after machining was studied. The prediction results of the deformation for the final parts were compared with the measured results after different heat

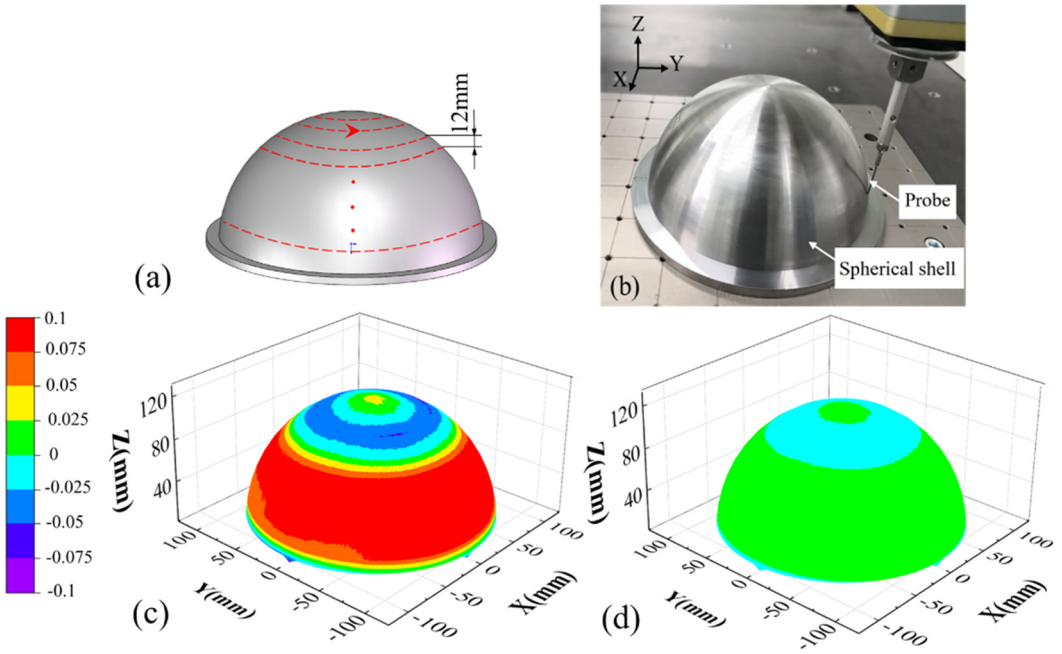

Figure 12: (a) Three-dimensional measurement path, (b) measurement setup, and the experimental measurement results (c) without and (d) with 650°C heat treatment.

treatment temperatures, as shown in Figure 14. The prediction results have a good agreement with the measured deformation from the experiments. With the increase in the heat treatment temperature, the deformation of the final parts after machining was decreased, which is attributed to the residual stress relaxation during the annealing. The predictive error might be attributed to the residual stress induced by machining, which led to a larger deformation in the experiments.

With regard to the grain size distribution, the maximum grain size of the semi-spherical shell was around 63 μm when the heat treatment temperature was lower

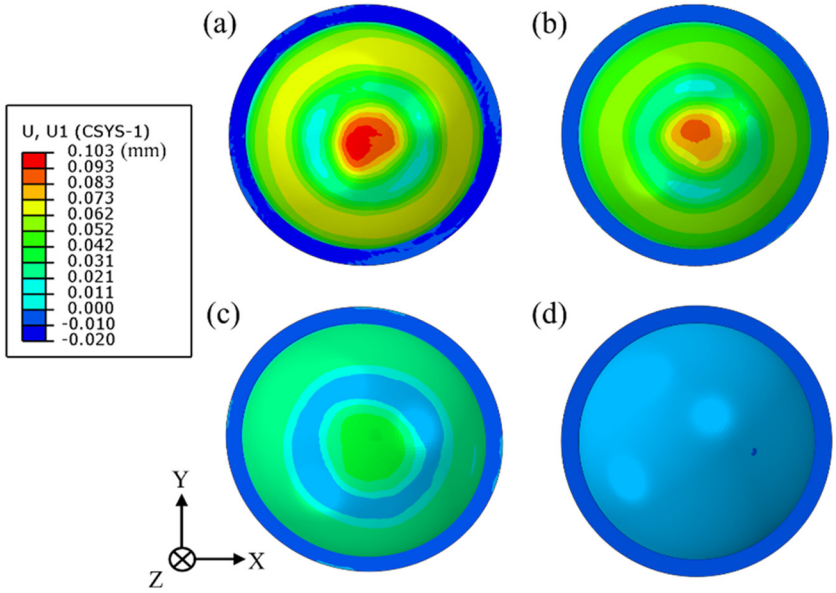

Figure 13: Simulated results of the deformation for the final part with different heat treatments: (a) without heat treatment, (b) with 500°C, (c) 600°C, and (d) 650°C heat treatment.

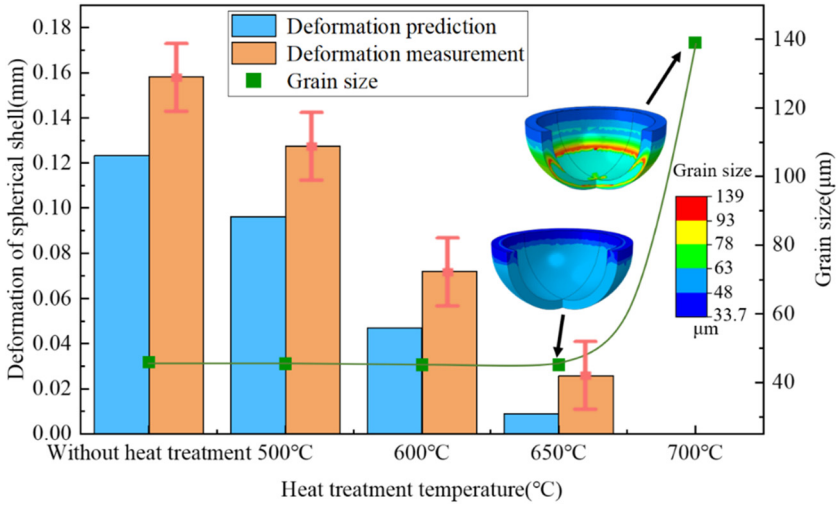

Figure 14: Experimental and simulated results of deformation and grain size for final parts with different annealing temperatures.

than 650°C, but the grain size was increased rapidly to 140 μm at a heat treatment temperature of 700°C due to grain growth, as shown in Figure 14. Therefore, the annealing temperature of 650°C was determined to eliminate residual stress as well as to obtain a uniform grain size distribution.

6 Conclusion

In this article, the residual stress change of a forged pure iron part in annealing heat treatment and material removal was investigated. A modified creep constitutive model with the consideration of microstructure evolution was established to describe the residual stress relaxation in the annealing. The grain size after the heat treatment was predicted and validated by the microstructure observation. The simulated deformation after machining had a good agreement with the experimental results. The key findings were summarized as follows:

1. The proposed stress relaxation model considered the effect of initial strain hardening and microstructure evolution, which could accurately predict the residual stress change during heat treatment.
2. The residual stress was indirectly evaluated by measuring the machining deformation of the thin-walled parts, which can be used as an effective method for the evaluation of the very low-level residual stress.
3. For pure iron thin-walled parts, the determined annealing temperature is 650°C, at which the deformation of the component was minimum and the grain size distribution was uniform.
4. The proposed method for the determination of heat treatment parameters could be applied to the thin-walled parts with other materials such as aluminum and titanium alloys.

Acknowledgment: The financial supports from the Science Challenge Project (JCKY2016212A506-0101) and the National Natural Science Foundation of China (52175381) are gratefully acknowledged.

Funding information: The Science Challenge Project (JCKY2016212A506-0101) and the National Natural Science Foundation of China (52175381).

Author contributions: Qian Bai: conceptualization, methodology and draft preparation. Ziliang Chen: methodology and draft preparation. Yingming Gao: conceptualization and methodology. Hang Li: methodology. Jingang Tang: investigation. All authors have read and agreed to the published version of the manuscript.

Conflict of interest: Authors state no conflict of interest.

Data availability statement: Not applicable.

References

[1] Wang, Z., W. Y. Chen, Y. D. Zhang, Z. T. Chen, and Q. Liu. Study on the machining distortion of thin-walled part caused by redistribution of residual stress. *Chinese Journal of Aeronautics*, Vol. 18, No. 2, 2005, pp. 175–179.

[2] Foss, B. J., S. Gray, M. C. Hardy, S. Stekovic, D. S. McPhail, and B. A. Shollock. Analysis of shot-peening and residual stress relaxation in the nickel-based superalloy RR1000. *Acta Materialia*, Vol. 61, No. 7, 2013, pp. 2548–2559.

[3] Wang, C., C. Jiang, and V. Ji. Thermal stability of residual stresses and work hardening of shot peened tungsten cemented carbide. *Journal of Materials Processing Technology*, Vol. 240, 2017, pp. 98–103.

[4] Wang, Z., A. D. Stoica, D. Ma, and A. M. Beese. Stress relaxation in a nickel-base superalloy at elevated temperatures with in situ neutron diffraction characterization: Application to additive manufacturing. *Materials Science and Engineering: A*, Vol. 714, 2018, pp. 75–83.

[5] Epp, J., H. Surm, T. Hirsch, and F. Hoffmann. Residual stress relaxation during heating of bearing rings produced in two different manufacturing chains. *Journal of Materials Processing Technology*, Vol. 211, No. 4, 2011, pp. 637–643.

[6] Radchenko, V. P., M. N. Saushkin, and V. V. Tsvetkov. Effect of thermal exposure on the residual stress relaxation in a hardened cylindrical sample under creep conditions. *Journal of Applied Mechanics and Technical Physics*, Vol. 57, No. 3, 2016, pp. 559–568.

[7] Dong, P., S. Song, and J. Zhang. Analysis of residual stress relief mechanisms in post-weld heat treatment. *International Journal of Pressure Vessels and Piping*, Vol. 122, 2014, pp. 6–14.

[8] Zhang, W., X. Wang, Y. Wang, X. H. Yu, Y. F. Gao, and Z. L. Feng. Type IV failure in weldment of creep resistant ferritic alloys: I. Micromechanical origin of creep strain localization in the heat affected zone. *Journal of the Mechanics and Physics of Solids*, Vol. 134, 2020, id. 103774.

[9] Zhang, W., X. Wang, Y. Wang, X. H. Yu, Y. F. Gao, Z. L. Feng. Type IV failure in weldment of creep resistant ferritic alloys: II. Creep fracture and lifetime prediction. *Journal of the Mechanics and Physics of Solids*, Vol. 134, 2020, id. 103775.

[10] Zhang, X. C., B. S. Xu, H. D. Wang, and Y. X. Wu. Residual stress relaxation in the film/substrate system due to creep deformation. *Journal of Applied Physics*, Vol. 101, No. 8, 2007, id. 83530.

[11] Hadadian, A. and R. Sedaghati. Investigation on thermal relaxation of residual stresses induced in deep cold rolling of Ti–6Al–4V alloy. *The International Journal of Advanced Manufacturing Technology*, Vol. 100, No. 1–4, 2019, pp. 877–893.

[12] Zhang, Z. *Research on residual stress and machining distortion of aeronautic weak rigidity in aluminum structure*, Nanjing University of Aeronautics and Astronautics, Nan Jing, 2015.

[13] Ajovalasit, A., G. Petrucci, and B. Zuccarello. Determination of nonuniform residual stresses using the ring-core method. *Journal of Engineering Materials and Technology*, Vol. 118, No. 2, 1996, pp. 224–228.

[14] Withers, P. J. and H. K. D. H. Bhadeshia. Residual stress. I – Measurement techniques. *Materials Science and Technology*, Vol. 17, No. 4, 2001, pp. 355–365.

[15] Bai, Q., H. Feng, L.K. Si, R. Pan, and Y. Q. Wang. A novel stress relaxation modeling for predicting the change of residual stress during annealing heat treatment. *Metallurgical and Materials Transactions A*, Vol. 50, No. 12, 2019, pp. 5750–5759.

[16] Gao, H., Y. Zhang, Q. Wu, and B. H. Li. Investigation on influences of initial residual stress on thin-walled part machining deformation based on a semi-analytical model. *Journal of Materials Processing Technology*, Vol. 262, 2018, pp. 437–448.

[17] Huang, X., J. Sun, and J. Li. Finite element simulation and experimental investigation on the residual stress-related monolithic component deformation. *The International Journal of Advanced Manufacturing Technology*, Vol. 77, No. 5–8, 2015, pp. 1035–1041.

[18] Zheng, J., J. Lin, J. Lee, R. Pan, C. Li, and C. M. Davies. A novel constitutive model for multi-step stress relaxation ageing of a pre-strained 7xxx series alloy. *International Journal of Plasticity*, Vol. 106, 2018, pp. 31–47.

[19] Estrin, Y. Dislocation theory based constitutive modelling: foundations and applications. *Journal of Materials Processing Technology*, Vol. 80, 1998, pp. 33–39.

[20] Frost, H. J. and M. F. Ashby. *Deformation mechanism maps: the plasticity and creep of metals and ceramics*, Pergamon Press, 1982.

[21] Sun, Z. C., H. Yang, G. J. Han, and X. G. Fan. A numerical model based on internal-state-variable method for the microstructure evolution during hot-working process of TA15 titanium alloy. *Materials Science and Engineering: A*, Vol. 527, No. 15, 2010, pp. 3464–3471.

[22] Kocks, U. F. Laws for work-hardening and low-temperature creep. *Journal of Engineering Materials and Technology*, Vol. 98, No. 1, 1976, pp. 76–85.

[23] Avrami, M. Granulation, phase change, and microstructure kinetics of phase change. III. *The Journal of Chemical Physics*, Vol. 9, No. 2, 1941, pp. 177–184.

[24] Siwecki, T. Modelling of microstructure evolution during recrystallization controlled rolling. *ISIJ International*, Vol. 32, No. 3, 1992, pp. 368–376.

[25] Lü, Y., D. A. Molodov, and G. Gottstein. Recrystallization kinetics and microstructure evolution during annealing of a cold-rolled Fe–Mn–C alloy. *Acta Materialia*, Vol. 59, No. 8, 2011, pp. 3229–3243.